AIAA Paper No. 98-0428

# Application of a Planar Doppler Velocimetry System to a High Reynolds Number Compressible Jet

Michael W. Smith
NASA Langley Research Center

36th AIAA Aerospace Sciences Meeting and Exhibit

January 12-15, 1998
Reno, Nevada

# Application of a Planar Doppler Velocimetry System to a High Reynolds Number Compressible Jet

Michael W. Smith*
*NASA Langley Research Center, Hampton, Virginia 23681*

**Abstract**

A Planar Doppler Velocimetry (PDV) system has been constructed and used to investigate the instantaneous turbulent velocity structure of a round high-speed compressible air jet with a low-speed co-flow. The exit condition was Mach=0.85 at ambient pressure, yielding a Reynolds number of about 650,000 on diameter. The PDV system was installed at NASA Langley Research Center in the Small Anechoic Jet Facility (SAJF), a chamber in which both the acoustic and aerodynamic properties of jets can be studied. For this test, the goal was to gather data which can be used to relate the turbulence structure of the jet to the levels and character of the acoustic noise produced by the jet.

The current PDV system can acquire single-velocity-component, single-shot, planar images (15 ns exposures) at 30 Hz. For this paper, the primary data set consists of 240 frames of velocity data acquired with both the jet and the low-speed co-flow seeded with light-scattering particles. Thus, velocities could be measured everywhere in the jet shear layer, both in the jet fluid and in the entrained co-flow. Some data were also taken with only the jet flow seeded. These provided mixing concentration images along with the reduced velocity fields. Other images were taken with only the co-flow seeded. These produced unique quantitative images of high speed entrainment.

Optical "laser speckle" noise is the largest source of random noise in pulsed PDV systems. Components for the PDV imaging system were specifically selected to minimize speckle noise. To reduce systematic velocity errors due to laser drift, a frequency monitoring reference leg with a temperature-tuned reference iodine cell, was employed.

In the course of this study, a novel flow seeder was developed. It enabled continuously variable seeding of the flow with particles of Sheared Pyrogenic Amorphous Hydrophobic Silica (SPAHS). The seeder comprised a dry fluidized bed hopper and a supersonic nozzle "pickup." Shearing action in the pickup dispersed the seed material in an exceptionally fine cloud (~0.3 micron). These particles followed the flow well, did not clump or cake on screens or model surfaces, and were not susceptible to evaporation. Because of the refractory nature of the particles, SPAHS seeding should also be applicable to anticipated future testing at high temperatures.

## I. Introduction

A number of researchers[1-5] have reported progress on the development of Doppler velocimeters which acquire velocity images on a plane in the flow. These systems are based either on Rayleigh or Mie scattering for signal generation and use either argon-ion CW (continuous wave) lasers or frequency-doubled Nd:YAG pulse lasers. Both schemes employ optical filters full of iodine vapor for velocity discrimination, although different spectral lines are used.

The Nd:YAG/pulse laser approach is more useful for the study of turbulent flows and other unsteady phenomena since it provides instantaneous (~15 ns) images of the velocity field. This work describes progress in the development of a previously reported[6] 30 Hz pulsed Nd:YAG-based Planar Doppler Velocimetry (PDV) System as well as its installation and testing in the Small Anechoic Jet Facility (SAJF) at NASA Langley Re-

*Aerospace Engineer, Hypersonic Airbreathing Propulsion Branch (AGDD), in collaboration with the Aeroacoustics Branch (FMAD)

search Center. The goal of the test program was to reduce measurement inaccuracies in the PDV measurement as applied to this particular facility/geometry, discover and resolve facility integration problems, and acquire data sets on a round, compressible, high Reynolds number (650,000 on diameter) jet that would be of use to both the turbulent mixing and acoustics communities.

## II. Apparatus

**Optical System:**

Figure 1 shows a schematic of the optical system. The light source is an injection-seeded 30 Hz pulsed Nd:YAG laser which is frequency-doubled by a harmonic generator crystal to produce approximately 100 mJ, 15 ns pulses at 532 nm. A small fraction of the beam is split off and sent to a frequency monitoring leg which uses both an etalon and a reference cell to determine relative and absolute positioning of the laser in frequency space (discussed in detail below). The primary beam propagated approximately 20 feet from the table to the laser-sheet-forming optics in the facility. An optical splitter system was used to create the reference/Doppler image pairs required for the PDV technique. Both images were captured on a single CCD camera. With one pair of images, a single velocity component could be measured. It is indicated by the arrow labelled $(\hat{o} - \hat{i}) \bullet \hat{V}$ in Fig. 1. Due to the propagation direction of the laser and the viewing angle of the camera, this component is at an angle of 45° to the jet axis. For centerline average data, the transverse velocity component is zero and the data can be compared directly to streamwise pitot velocities or streamwise core velocities based on isentropic expansion (as will be done in Section III).

For the current implementation of the PDV system, three important changes were made to improve measurement accuracy. First, a different detector was used for the imaging. The two images required to determine the single velocity component measured were acquired side-by-side on a Cohu 4800 frame transfer CCD using optical splitters. This camera employed a Texas Instruments TC-241 array, a nearly 100% fill factor 2/3 inch format (8.8mm x 6.6mm active area) frame transfer chip. Laser speckle is the largest source of random error in PDV imaging and the best way to reduce it is to use the largest possible chip with the largest possible fill factor. Larger pixels provide better averaging of speckle patterns and lower speckle noise. At about $1000 per unit, TC-241 based cameras are an economical choice (as opposed to $25,000 scientific grade cameras) and a great improvement over more common 1/2" format interline chip cameras which have fill factors of less than 50%.

The second improvement was to use a more appropriate imaging lens, again to reduce laser speckle noise. Speckle noise increases linearly with f-number, so a "fast" lens is desirable. A 50 mm focal length 35 mm format f1.2 Nikon, a relatively low f-number, economical, and readily available lens, was employed. For all tests the aperture was left at the widest setting and exposure was controlled with laser intensity and flow seed density.

With this combination of lens and camera, a relatively low value of speckle noise, about 2% RMS, was achieved on the Doppler and reference images. If the noise between the Doppler and reference images were perfectly correlated (i.e. there was pixel-for-pixel correspondence) then all speckle noise would cancel. At the other limit, if the speckle noise between the two images was completely uncorrelated, the noise signals could be considered independent random variables and the variances would add. The RMS would then be:

$$\begin{aligned} RMS_{velocity} &= \sqrt{RMS^2_{Doppler} + RMS^2_{reference}} \\ &= \sqrt{2^2 + 2^2} \\ &= 2.8 \end{aligned}$$

The actual noise level for these velocity images was ~3% RMS, indicating that the noise was not correlated in this case.

One additional means of speckle noise reduction was tried but proved less effective than hoped and rather impractical. It was shown in tests with a laser sheet in a stationary sample medium, that when injecting two separate laser sheets, the imaged speckle noise could be reduced by a factor of $\sqrt{2}$. The sheets had to be separated in time by at least the width of the laser pulse (here generated with a single laser and an optical delay line) and separated in space by at least the width of the laser sheet. Reduction was achieved by imaging the superposition of the two uncorrelated speckle patterns generated by the two different laser sheets. In the SAJF test environment, half of the light passed to the sheet-forming optics was split off and run through a 20 meter delay line before it too was sent to the sheet-forming optics. It was hoped that the movement of the flow between laser pulse arrivals would sufficiently decouple the speckle patterns resulting in the same factor of $\sqrt{2}$ reduction in speckle noise seen in the stationary test. Instead, the resulting images displayed speckle noise with less than a 10 percent noise reduction. The images appeared "smeared" in the direction of motion by a fraction of a pixel, i.e. the amount the flow moved between the arrival of the first laser sheet and the second. This indicated that the desired decorrelation between the two speckle patterns was not realized. The additional experimental complexity associated with a long optical delay line was not warranted for the amount of noise reduction achieved; therefore, the

scheme was abandoned.

The third improvement was the addition of a frequency monitoring cell. A small fraction of the 532 nm laser beam was split off and passed down a referencing path and through a reference iodine cell. Photodiodes before and after the cell were used to monitor the relative transmission through the iodine vapor. Signals from the photodiodes were processed by boxcar integrators, the outputs divided on an analog module, and the resulting transmission ratio displayed in real time. By carefully selecting the proper temperature for the reference cell, the displayed ratio could be made highly sensitive to drifts in the laser frequency away from the set point desired for the experiment.

Figure 2 shows the calibration curve of the reference cell plotted with the calibration curve for the imaging cell. Both curves are representations of the iodine absorption line at 18787.8 $cm^{-1}$. These calibrations were done by scanning the laser at a fixed rate with the iodine cell (either the reference or imaging cell) placed in the referencing path described above. In this case the photodiode signals recorded the relative transmission ratio as a function of laser frequency.

Also plotted in Fig. 2 is the output from a 1 GHz free-spectral-range Fizeau etalon used to calibrate the relative scale of the frequency axis. Another small fraction of the 532 nm beam was split off, expanded to fill the aperture of the etalon (~25 mm), and passed through the etalon to a screen. A set of parallel interference fringes traversed the screen as the laser frequency was varied with time. Whenever a fringe advanced past a mark on the screen, a button connected to a battery was depressed to record a spike on a separate channel of the digital acquisition system. Ideally, this spike would have been recorded by letting the fringe traverse across the face of a photodiode, but no additional boxcar integrator channels were available.

Both cells had a pathlength of 20 cm and zero buffer gas partial pressure (i.e. pure iodine vapor). The imaging cell stem temperature (35 °C) and body temperature (70 °C) were regulated by PID controllers driving electric heaters with feedback from thermocouples on the cell. The body of the reference cell was maintained at 40 °C by the same means. However, the stem of the reference cell was held at 17 °C using a copper coil heat exchanger in a chiller circuit. This additional complexity was required because the desired reference stem temperature was below ambient.

Note that in the vicinity of the laser frequency set-point indicated on Fig. 2, the reference cell scan has a large slope while the imaging cell scan is nearly flat. If the reference cell conditions had been chosen to be the same as the imaging cell conditions, very little sensitivity to frequency drift would have been produced at this set-point. However, by cooling the reference cell stem, the spectrum was modified to yield a larger slope in the region around the set-point; thus, good sensitivity to laser drift was achieved. Based on the displayed drift error, the laser frequency was manually adjusted during jet data acquisition sessions by making corrections on a precision voltage source which supplied a signal to the temperature controller feedback circuit on the seed laser. Using this approach, slow (~ 5 MHz/minute) drifts away from set-point could be corrected prior to data acquisition, which only lasted about 4 seconds for a 120 image sample.

Related to this improvement was a modification of the laser to reduce short term frequency drift. Output frequency was found to be a strong function of laser rod temperature; thus, the original equipment temperature controller, a self-regulating thermal valve that metered flow of tap water through a heat exchanger in the laser's de-ionized cooling water circuit, was upgraded. The OEM valve was replaced with a stepping-motor driven valve controlled by a microprocessor PID unit which sensed rod temperature via a thermocouple in the laser's cooling water reservoir. To get maximum stability, the PID controller was run in proportional mode with manual offset, reducing temperature fluctuations to about +/- 0.1 K. This reduced laser frequency fluctuations due to rod cooling to below those introduced by seeder dither (~10 MHz).

This temperature control scheme also allowed variable control of the rod temperature. The Continuum YG-590 used for the current tests had better seeding stability at a rod temperature of 45 °C as opposed to the fixed factory-set value of about 41 °C.

**Flow Seeder:**

A unique flow seeder was developed in the course of the investigation. It produced Sheared Pyrogenic Amorphous Hydrophobic Silica (SPAHS) particles about 0.3 micron in size and with sufficient volume to obtain high SNR (signal-to-noise ratio) reference and Doppler images at the available laser energy (~25 mJ/pulse). The shearing, which occurred in the supersonic injector nozzle of the seeder described below, dispersed the seed. The bulk seed material, trade name Aerosil R972 (Degussa Corporation), is a pyrogenically produced (silane flame), amorphous synthetic silica which is post-processed through chemical treatment to be hydrophobic. It is an inert substance used as an additive in foods, beverages, paints, plastics, and rubber. Crystalline silica particles produce silicosis, or 'Quartz Lung,' but SPAHS, having an amorphous structure, presents no such hazard.[7] Since it is hydrophobic, SPAHS is very resistant to caking and agglomerating, and the raw material

(before shearing) is easily fluidized–a critical property for the current delivery scheme.

At $150 per 20 kg. bag, the Aerosil material was extremely economical. The approximate seed usage rate was just under 2 g/sec for the Mach=0.85 case (main jet air flow was about 300 g/sec).

A schematic outlining the operation of the SPAHS seeder is shown in Figure 3. Fluidizing air is introduced through line A to the chamber at the base of the seed hopper C. The air passes through membrane B (a plastic fiber cloth) and lifts the bulk seed material from the membrane into a "fluidized" slug of freely suspended air/seed mixture. Valve D at the top of the hopper can be adjusted to limit the venting of the fluidizing air, thus pressurizing the seed hopper to produce higher seed flow rates as necessary. The seed hopper is constructed of clear plastic pipe, allowing the operator to visually observe the height of the fluidized seed column. Thus the pressure at A and the back pressure induced by D can be balanced to produce the desired result (sufficient "fluffing" without overflow of seed through the vent at the top of the hopper).

The seed flow air is introduced on high pressure line E (75 - 100 psia for the current tests), passes through the seed pick-up and is carried to the jet core flow and co-flow by the exhaust line F. On the inset diagram, the details of the seed pick-up are shown. The body of the pick-up is a Mach 3 converging-diverging nozzle. Seed is introduced into the pick-up body through a normal injector J (a hole drilled at a right angle to the Mach 3 air stream). The injection port is normally closed by the insertion of the shut-off valve H. This valve is only opened by the pneumatic actuator G when seed is required. Typically, the fluidizing flow (A→D), the seed flow (E→F), and the facility flow are all established and equilibrated, a process that may take several minutes, before valve H is opened just prior to data acquisition.

Prior to passage through the injector port, the seed consists of "feathers" of silica particles (approximately 0.016 μm in diameter[8]) loosely bound into long interwoven chains (~ 500 μm across). When the seed feathers are drawn into the port J, they experience a cross flow of approximately 600 m/sec and are powerfully sheared into smaller particles. Further dispersion is presumed to take place in the shock train downstream of the pressure mismatched Mach 3 nozzle. A typical particle size of 0.3 μm was observed for samples deposited on a slide and viewed under an optical microscope.

**Small Anechoic Jet Facility (SAJF):**

The SAJF is an approximately 7x10 meter anechoic chamber in which both the acoustic and aerodynamic properties of free jets can be studied. Figure 4 illustrates the jet hardware as installed in the chamber. The main jet air was supplied from a central 1000 psi air supply and could be electrically heated to high temperature (in the current tests just 305 K to reduce condensation on the hardware).

Prior to the current test, the facility had undergone an ad-hoc modification to provide some variety of co-flow. A two foot diameter sheet metal pipe allowed room air to be drawn into the chamber around the jet piping. An exhaust blower at the far end of the chamber induced a co-flow of about 7 m/s. Turbulence levels in this flow were so high due to the wake from the jet hardware supports and the massive leading edge separation from the straight sheet metal pipe, that it was not possible to produce a uniform region of seed around the central jet. A temporary bell mouth (flashing and tape) and a temporary centerbody (corrugated cardboard and tape) were constructed at the inlet of the two-foot diameter pipe. Turbulence screens were also added at downstream locations to further stabilize the co-flow. With the bulk co-flow settled, it was then possible to velocity match an inner annulus (about 1 inch in the radial direction) of seeded co-flow air and have it delivered in a uniform field to the jet exit. This air was supplied by a variable speed centrifugal blower. The SPAHS seed was added just upstream of the blower to ensure good mixing of the injected seed with the co-flow air. For the central jet, seed was simply injected through a single port in the main supply pipe just upstream of the co-flow inlet.

The laser table with monitoring/calibration optics and the other data acquisition equipment were located adjacent to the anechoic chamber in a controlled access partition area. From the partition area, the laser beam was passed through a protective pipe enclosure to a 12 cm. hole in the wall of the anechoic chamber. Inside the chamber, the beam was steered by a turning prism to laser-sheet-forming optics on a rail parallel to and beneath the jet centerbody. Finally, as shown in Fig. 4, the laser sheet was turned up by a mirror to the airfoil-enclosed periscope which injected it upstream into the flow by means of another mirror and a window in the leading edge of the airfoil. Attached firmly to a 2 foot x 6 foot optical table which was in turn secured to a heavy metal translation system on the floor of the chamber, the airfoil periscope isolated the enclosed optics from the dynamic loads imposed by the jet flow.

The beam path throughout the anechoic chamber was completely enclosed, either with plastic PVC piping or sheet metal box covers, to prevent seed material from settling on optical surfaces. The most vulnerable part of the enclosure was the leading edge of the airfoil. Here, an uncoated glass window was secured with silicone sealant over a 1 cm wide slit which had been milled to pass the

laser sheet upstream into the flow. Care was also taken to tape over all the other joints around the leading edge of the periscope enclosure–in an early trial SPAHS seed was driven in through a narrow seam in the metal skin and coated all the optics.

An initial concern, that air film injection would be required along the leading edge to keep the window clear of deposited seed, proved unfounded. With the non-caking SPAHS, the window was easily kept clear by the force of the impinging jet flow.

## III. Data

The raw data set acquired in this experiment consists of 240 reference image/Doppler image pairs taken at 30 Hz in the M=0.85 round jet. All data were acquired on a vertical centerline plane and include a streamwise extent of just over 6 jet diameters. Each image contains 580 pixels in the streamwise direction and 120 in the transverse direction for a total of 69,600 sample locations.

For a comparison of this resolution to more conventional measurement technology, consider an equivalent normal hot-wire frequency response that can be calculated using the mean flow velocity and Taylor's hypothesis. In other words, if the turbulence structures seen on the PDV images did not evolve but simply translated over an ideal hot-wire, what frequency response would be required to provide the same spatial resolution seen on the images? Assuming 2x2 pixel binning for a conservative estimate of spatial resolution, and a jet core flow of 280 m/s, this value is about 400 kHz.

It should be noted that this 400 kHz equivalent response is only valid to the local region of each image. Because the images were acquired at 30 Hz and the flow moves much more than 6 diameters between images, each image is an independent random sample. There is no temporal overlap between images (as would be required to make a true "movie").

Figure 4 shows a typical set of images acquired in a single laser pulse. The reference and Doppler images were acquired simultaneously on the camera; the velocity image was derived using the following method:

1. A background file was generated by blocking the laser and sampling 100 images which were averaged together. This background file was subtracted from each gain, reference, and Doppler image prior to further processing.

2. A 'gain' file was generated by steering the laser beam onto a white card placed near the camera. Laser light scattered from the card illuminated a poster board screen placed 20 cm beyond the jet centerline (this kept the imperfections on the poster board out of focus). The image of this uniform field of light recorded the vignetting introduced by the splitter optics and iodine cell and the gain for each camera pixel. Each data frame was divided by this gain image to remove these effects.

3. The processed Doppler image was extracted from one side of the frame and slightly warped using bilinear interpolation to register exactly with the other side of the frame. It was found that registration accuracy to a tenth of a pixel or less was required to provide good velocity images. Warping 'tie-points' were determined interactively by aligning a 'dots' file. This image was produced by blowing dust into the measurement volume with the laser sheet on to produce a field of pixel-sized dots that were suitable for alignment.

It should be noted that a dot imaged on the reference half of the CCD might be centered on a pixel, while on the Doppler half of the array the light from that dot might be split over two or more neighboring pixels. When selecting tie points for the registration warp, every effort was made to select, with subpixel accuracy, the centroid of each dot when it occupied more than one pixel.

4. The processed Doppler image was divided by the processed reference image and the ratio converted from intensity to velocity using the transmission curve in Fig. 2. Dither noise was removed from the transmission curve by loose fitting a spline. It should be noted that velocity is set to zero in regions where the reference image signal is too low to produce good data (say, 50 counts). Thus, in regions of the flow with little or no seed, velocity is automatically (if not necessarily correctly) set to zero.

This data reduction process was performed using in-house C routines object-linked via command line arguments in UNIX shells. By using these optimized routines and a low-overhead raw data format, a data reduction speed of about ten velocity images per minute was achieved on a relatively slow DecStation 5000.

For Fig. 5, SPAHS seed was added only to the jet fluid. Although not the optimum strategy for measuring the velocity field, the reference image for this arrangement provides a good mixing map of the jet fluid as it spreads into the co-flow air. Variations in intensity across the laser sheet have not been removed, so this mixing map is only an approximation. The dark stripe down the jet centerline is an artifact due to a non-uniform laser sheet, although note that it is completely removed in the final velocity image via the ratio step in the data reduction process. Compare the reference and velocity image. On

the reference image, intensity is linearly related to jet fluid density; on the velocity image, intensity is linearly related to velocity (the brightest regions are at about 280 m/sec). The spreading rate in the reference image is larger as jet mass is stripped off and fills a rotational layer between the instantaneous potential core and the co-flow. In the velocity image most of this rotational fluid is not visible, indicating that it is travelling at quite a low speed (under 50 m/sec). However, some 'fingers' of high speed fluid, inclined to the jet axis at about 45°, persist.

In Fig. 6 SPAHS seed has been introduced to both the jet flow and the co-flow. This is the optimal arrangement for velocity imaging since velocities can then be determined everywhere in the field, in the entrained as well as the entraining air. The primary data set of 240 velocity images was taken with this seeding scheme. The main difference between Fig. 6 and Fig. 5 is that the co-flow is visible in the reference image in Fig. 6. The corresponding Doppler images look very similar, but in Fig. 5 the co-flow region outside the central jet is dark because there is no seed there; in Fig. 6 it is dark because the light scattered from it is suppressed by the velocity discriminating filter. This is an important distinction. In Fig. 6, the Doppler image should contain more information, namely signal from the fluid elements which have been accelerated by the jet but have not mixed fully with jet fluid.

In Fig. 7, SPAHS seed has been added only to the co-flow fluid, producing unique visualizations of the entrainment process. Doppler images are shown for two cases: the same M=0.85 flow condition represented in the previous figures, and a supersonic screeching case. The supersonic screech case was achieved by using the same converging nozzle and increasing the nozzle pressure ratio (NPR) to a value that would produce M=1.2 were the flow perfectly expanded.

In Doppler images, greyvalue at any pixel is a function of two things, seed density and velocity. For Fig. 7, only fluid elements which have come from or mixed with elements from the co-flow contain seed; only fluid elements which have been accelerated appear bright through the velocity discriminating filter. To the extent to which the co-flow is seeded uniformly and to which the velocity discriminating filter is linear, these images represent the product of co-flow fluid concentration and velocity. This quantity is an excellent indicator of entrainment and mixing.

In Fig. 7 there are structural differences in the character of the subsonic and supersonic mixing streams. The overall spreading rate of the subsonic layer is somewhat lower, although in the first diameter of streamwise progress the rate is higher. In Fig. 8 an expanded view comparison of this initial part of the shear layer shows the characteristically lower spreading rate of the supersonic case. Also, note the obvious differences in shape and periodicity of these initial shear layer instabilities. Farther downstream, the supersonic layers spread more quickly and develop periodic packets of entrainment associated with screech. A typical packet spacing is about 1 jet diameter, which implies a screech tone of about 8 kHz for a packet translation speed of 280 m/s.

Some statistical results are presented in Fig. 9. A mean and RMS velocity image for the data set with simultaneous jet/co-flow seeding are given, as well as a mean image for the case with co-flow seed only. Each image is based on a 240 shot data set.

For the purpose of quantitative comparison, selected one-dimensional velocity profiles have been extracted from the images at three stations as indicated on the mean image in Fig. 9. These are presented in Figs. 10 a-c. At each station three profiles are given, one from each image–namely, the mean velocity profile, the RMS profile, and a mean velocity profile based on the data set where only the co-flow contained seed. On each plot the expected core velocity based on isentropic expansion is indicated for comparison. The measured velocity component is actually at 45° to the jet axis; however, for a plane on the centerline of the axisymmetric jet, the mean cross-stream velocity component can be assumed zero, allowing this comparison.

At Station 1 the average core velocity agrees well with that for isentropic expansion, although the exit velocity is not uniform. A somewhat higher velocity at the top of the jet (~10%) is believed to be due to the removal of some flow conditioning elements in the jet plenum. By Station 3 the jet has spread and equilibrated, producing a highly symmetric average profile.

From the RMS profile at Station 1, fluctuations across the jet exit are about 18 m/s, or about 7% of core velocity. Approximately 3% of this RMS is an artifact due to laser speckle noise. The remainder is assumed to be due to laser dither and actual jet core velocity fluctuations. In the shear layers, the peak RMS values at Station 1 are about 33% of the core velocity. As the layers thicken, the peak RMS values decrease to about 18% by Station 2. By Station 3, the shear layers are beginning to merge (at least in the mean) and the peak RMS values rise slightly to about 22% of core velocity.

Although the RMS profiles are fairly smooth, a careful inspection of the RMS image in Fig. 9 shows that at 240 samples, convergence has still not been achieved. Interestingly, the image shows some "grain" in the shear layers, inclined to the jet axis at about 45°. This suggests that the prime contributors to the RMS field are turbulence structures of that orientation.

The mean velocity profiles based on co-flow-only seeding for Stations 1, 2 and 3 (indicated as "co-only" in

Figs. 10 a-c) agree well with the actual (seed both streams) mean velocity profiles at the outer edge of the shear layers. This region of agreement is small at Station 1 but grows as the shear layer thickens until Station 3, where over half of the shear layer velocity profile is captured with co-flow-only seeding. It is presumed that over the region of agreement, only velocity fluctuations due to the growing rotational layer of fluid between the co-flow and potential core are important. At the inner edge of this region, the velocity based on co-flow only seeding becomes invalid, dropping off as the intermittent instantaneous potential core comes into play. There is essentially no seed in the potential core since the only transport mechanism to get it there is molecular diffusion, which is insignificant compared to turbulent diffusion at these flow conditions. Recall that the data reduction algorithm assigns a velocity value of zero (incorrectly, in this special case) to any region where there is little or no seed.

Figure 11 directly compares the mean velocity profiles at Station 3 for the case with jet-only seed, co-flow-only seed, and seed in both streams (the assumed best answer). Note that the jet-only-seed profile is in near perfect agreement with the profile for both streams seeded. This should come as no surprise after viewing Fig. 5, where the reference image shows a faster spreading rate than the Doppler image–the implication being that all the important velocity fluctuations are marked by seed from the jet core.

The most interesting comparison in Fig. 11 might be that between the profile with co-flow-only seeding and the profile with jet-flow-only seeding. These agree over the same rotational part of the layer that was previously discussed. Thus it is interesting to note that over this substantial region of the shear layer, the same velocity profile is achieved whether the seed is put just in the central jet or just in the co-flow.

Pitot profiles of this jet were available from a previous test series, but not for the same total temperature condition. However, a pitot profile for Station 3 at $T_0$=445 K, which has been scaled according to centerline velocity, is plotted with the corresponding PDV data in Fig. 12. These profiles show excellent agreement in overall shape with some disagreement in the wings. The PDV data show a more gradual transition to zero velocity in the wings, a more "physical" result.

## IV. Conclusions

An improved PDV system was installed and demonstrated in the Small Anechoic Jet Facility (SAJF) at NASA Langley Research Center. Data suitable for both acoustic and mixing analysis were generated on the centerline plane of a Mach=0.85 round compressible jet. A reference iodine cell monitoring system was used to reduce systematic velocity errors due to laser frequency drift and an improved imaging system reduced random velocity errors due to speckle noise.

A novel "SPAHS" flow seeder was developed for these tests. It generated a relatively large volume (compared to PIV or LDV) of relatively small seed (~0.3 micron) which did not clog the plumbing or coat the window on the leading edge of the periscope airfoil used to inject the laser sheet up the jet centerline. Innovations in the seeder design allowed precise control of the seed density, allowing the seed flow rate to be used as the imaging exposure control. This was critical to reducing the experimental complexity since the laser operated best at one power setting (maximum) and the imaging lens had to be used at one aperture setting (full open to reduce speckle).

Mean and RMS velocity images and sample instantaneous velocity images were presented for selected cases where only the jet was seeded, only the co-flow was seeded, and both the jet and co-flow were seeded. Unique visualization images of mixing and entrainment were generated in the case of co-flow-only seeding.

Sample transverse velocity profiles were extracted from the mean and RMS images and plotted for quantitative comparisons. These profiles showed that for the region of this jet that was examined (just over 6 diameters streamwise) the mean velocity profiles were the same whether the co-flow was seeded or not. At the farthest downstream location, the velocity profiles based on co-flow-only seeding agreed with the correct profile over a large part of the shear layer. This zone of agreement indicates where, on average, mixing between the core and co-flow has occurred.

The quantitative accuracy of the mean velocity data was corroborated both by comparison to core velocity based on isentropic expansion from measured plenum conditions, and by comparison to pitot measurements at the downstream station. The RMS velocity data were in reasonable ranges although no facility-specific data were available for comparison. A base level for RMS noise of about 3% was observed and attributed primarily to laser speckle.

## V. References

[1]Komine, H., Brosnan, S. J., Litton, A. B., and Stappaerts, E. A., "Real-Time, Doppler Global Velocimetry," AIAA paper 91-0337, Jan. 1991.

[2]Meyers, James F., "Development of Doppler Global Wind

Tunnel Testing," AIAA paper 94-2582, June 1994.

[3]McKenzie, R. L., "Measurement Capabilities of Planar Doppler Velocimetry Using Pulsed Lasers," AIAA paper 95-0297, Jan. 1995.

[4]Clancy, P., Kim, J.–H., and Samimy, M., "Planar Doppler Velocimetry in High Speed Flows," AIAA paper 96-1990, June 1996.

[5]Forkey, J.N., Finkelstein, N.D., Lempert, W.R., and Miles, R.B., "Control of Experimental Uncertainties in Filtered Rayleigh Scattering Measurements," AIAA paper 95-0298, Jan. 1995.

[6]Smith, M.W. and Northam, G.B., "Application of Absorption Filter–Planar Velocimetry to Sonic and Supersonic Jets," AIAA Journal, Vol 34, No. 3, March 1996.

[7]"Technical Bulletin Pigments: The Biological Effects of $SiO_2$, $Al_2O_3$ and $TiO_2$", Number 64, Degussa AG, Geschäftsbereich Anorganische Chemieproduckte, Federal Republic of Germany, Printed July 1992.

[8]"Technical Bulletin Pigments: Basic Characteristics of AEROSIL®", Number 11, Degussa AG, Geschäftsbereich Anorganische Chemieproduckte, Federal Republic of Germany, Printed August 1993.

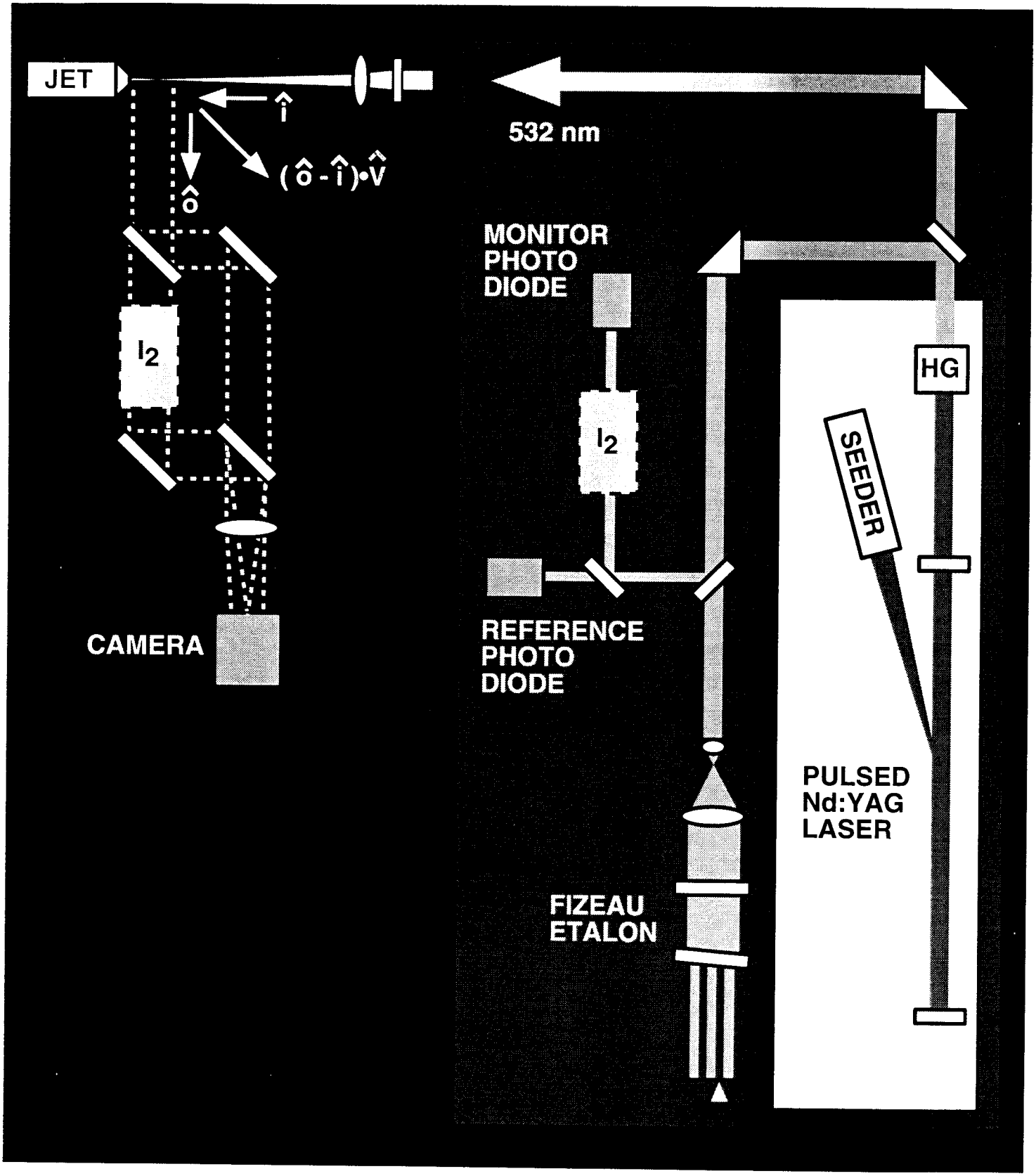


Fig. 1 PDV Apparatus Schematic

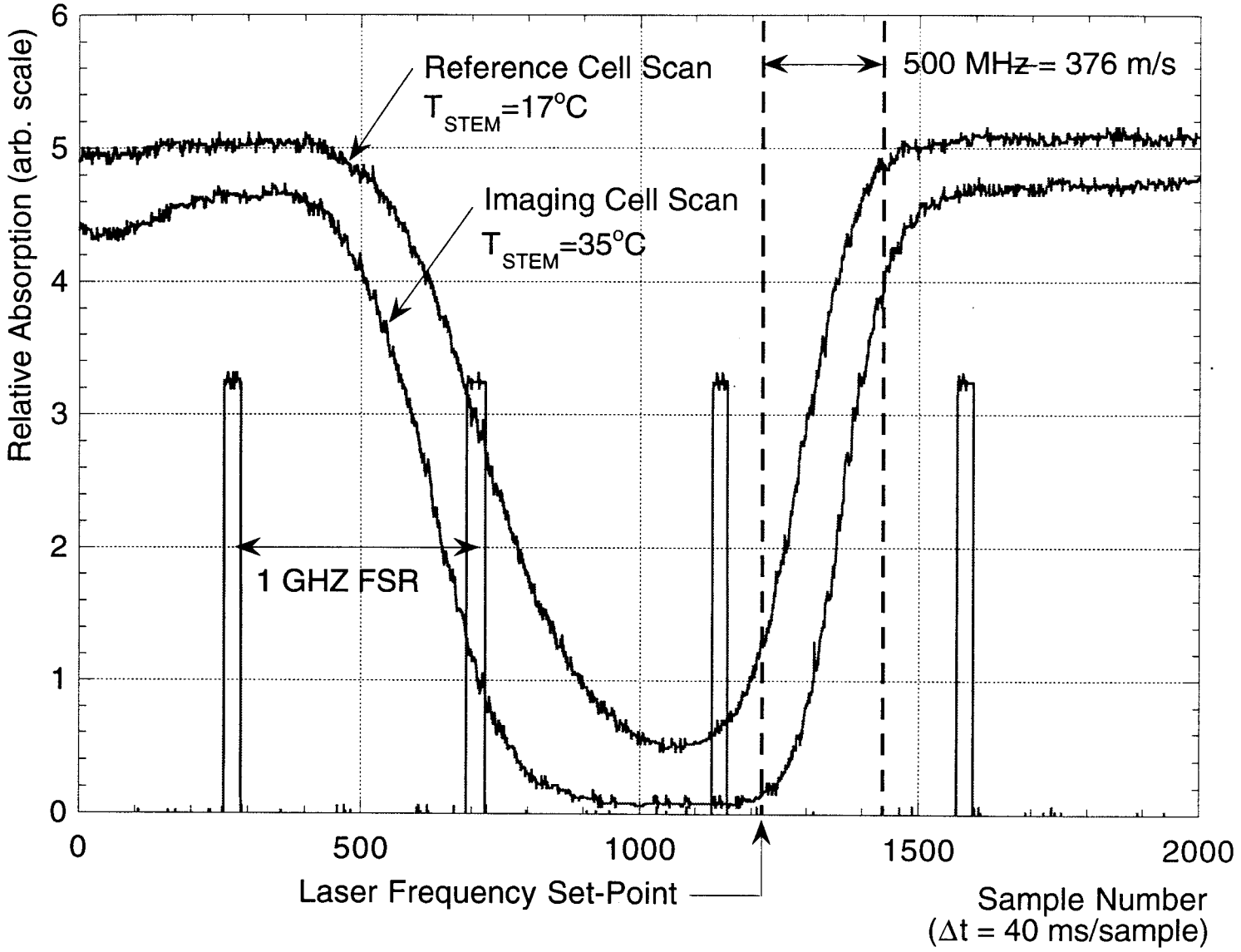


Fig. 2 Absorption Scans for Reference and Imaging Iodine Cells

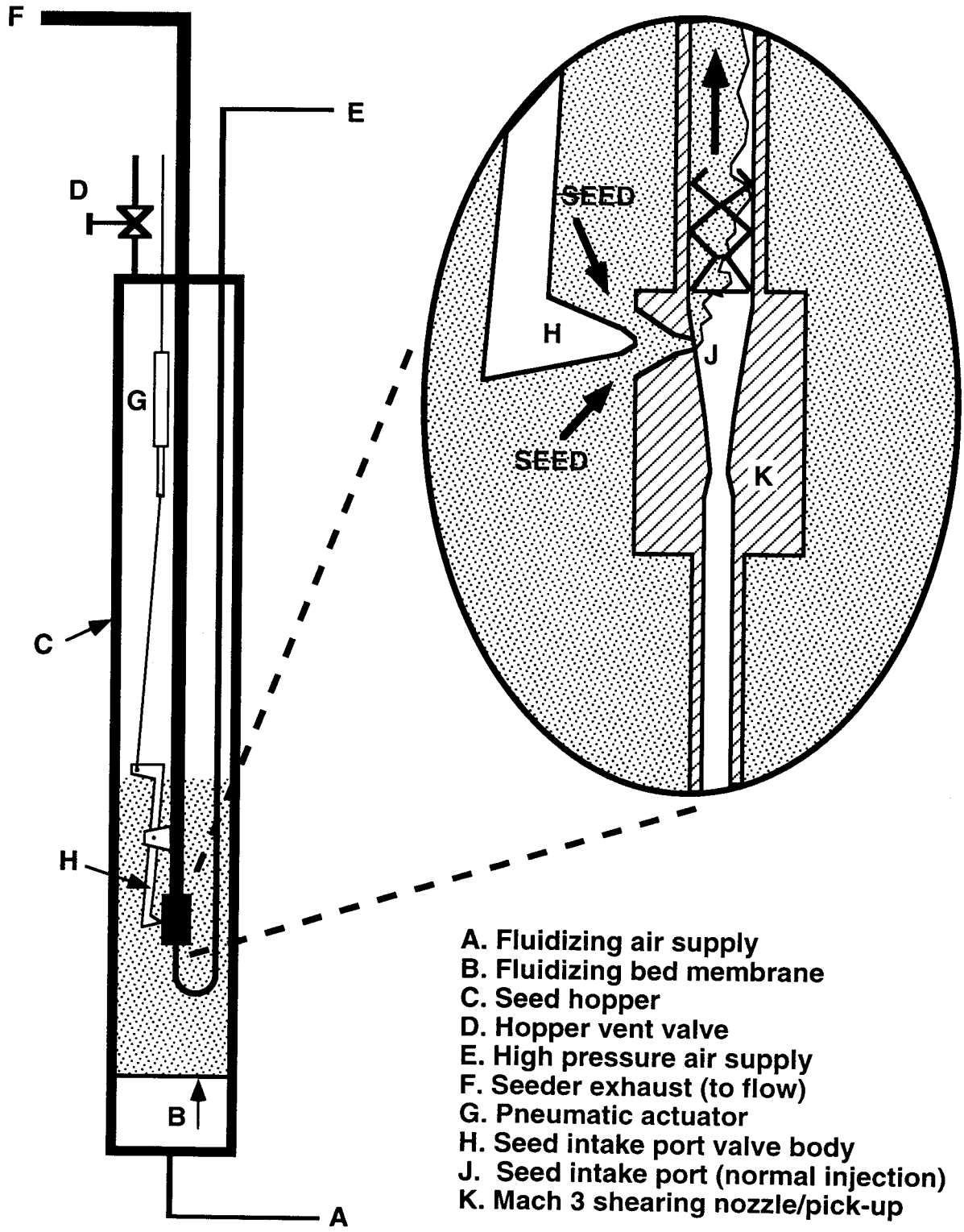


Fig. 3 SPAHS Dry Powder Seeder Schematic

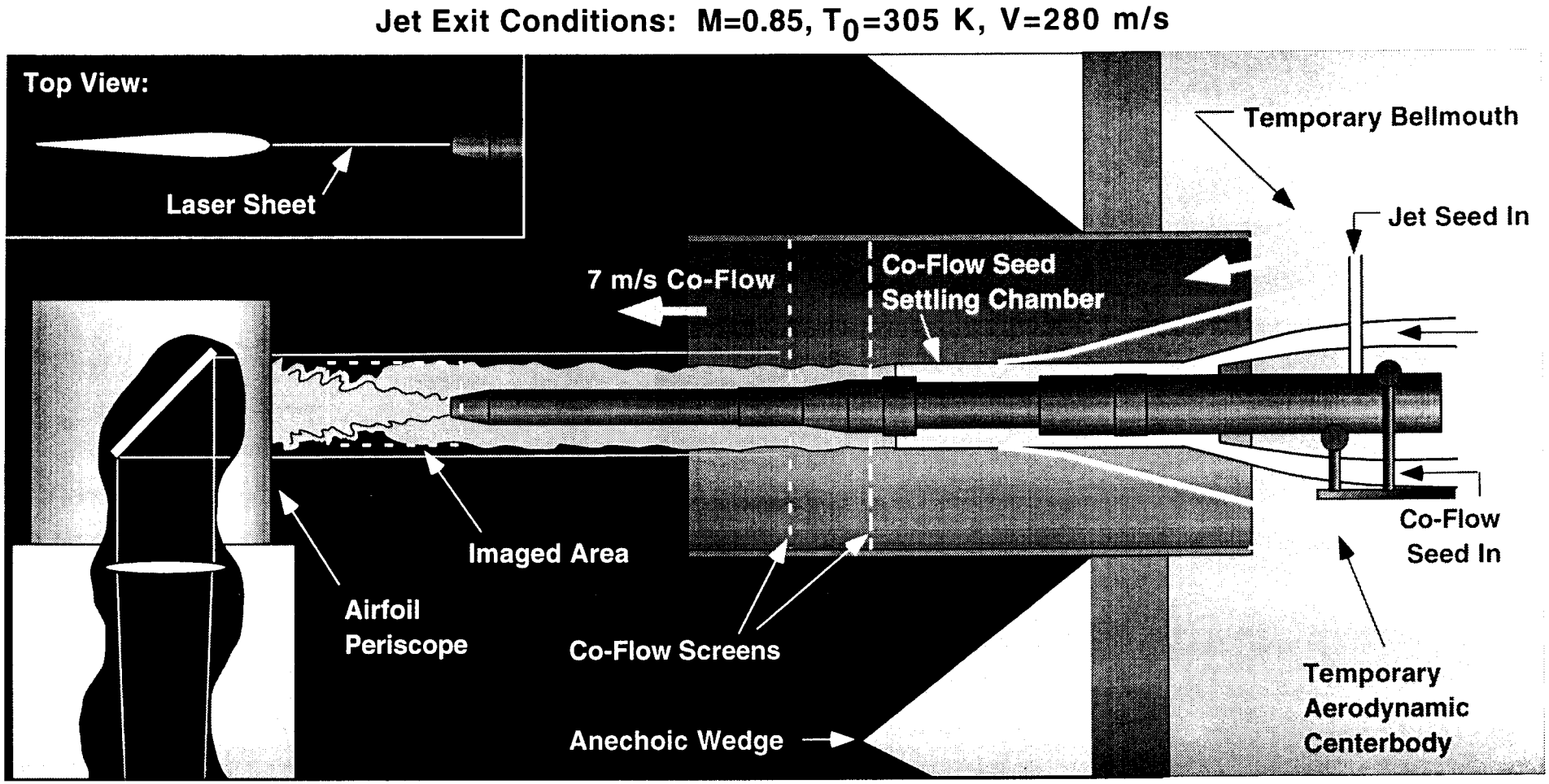


Fig. 4 Schematic of Small Anechoic Jet Facility (SAJF) Nozzle with Flow Seeding and Optical System

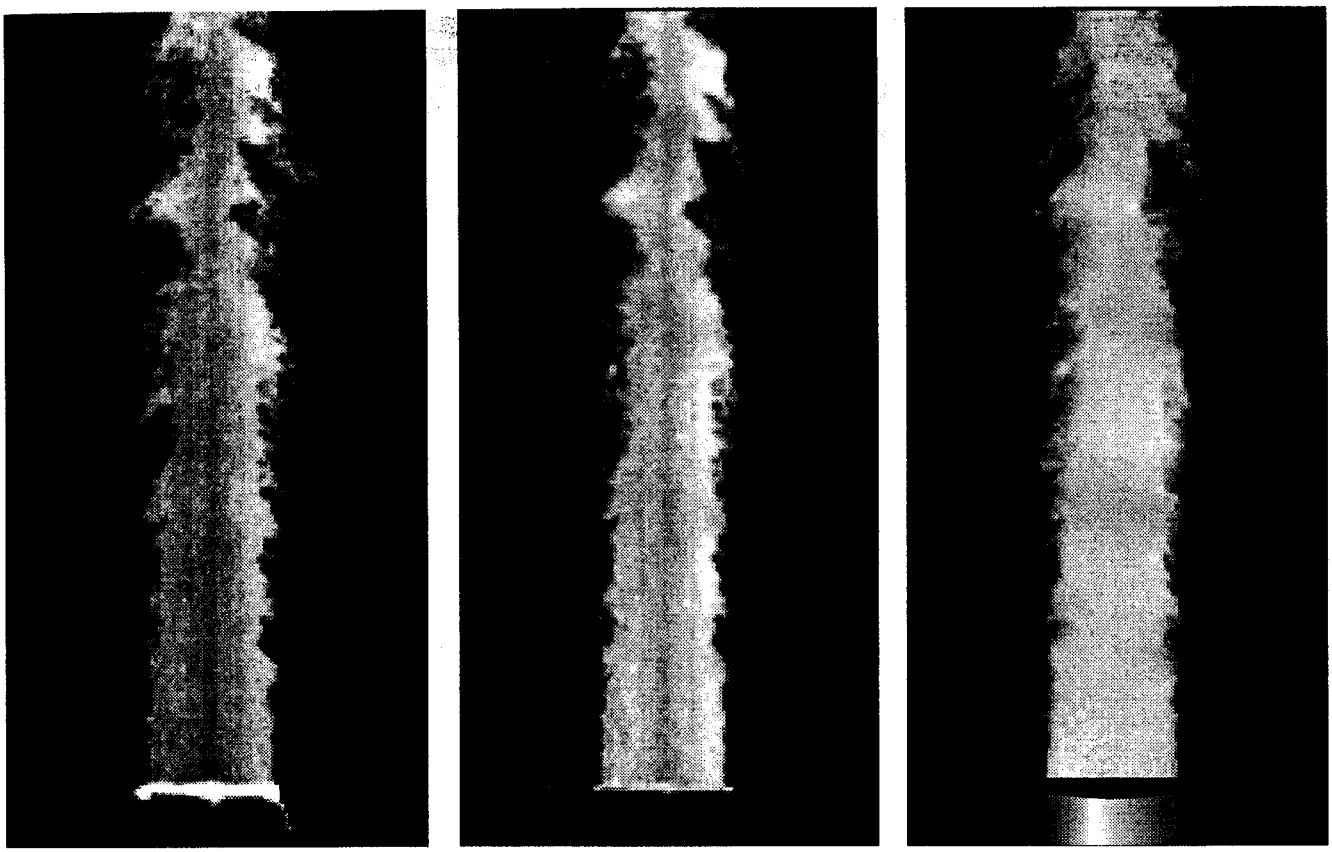


Fig. 5 Mach=0.85 Compressible Air Jet,
SPAHS Seed in Jet Fluid Only

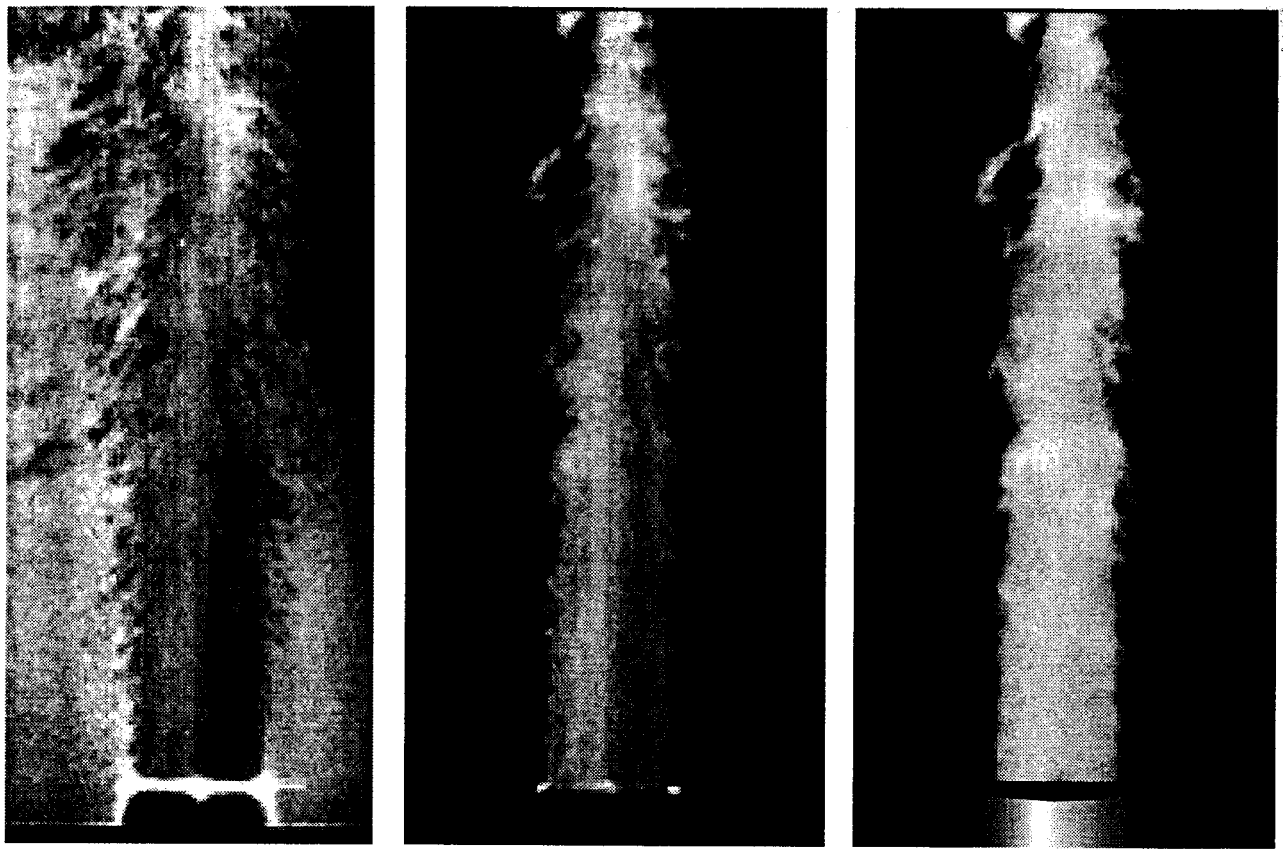


Fig. 6 Mach=0.85 Compressible Air Jet,
SPAHS Seed in Both Jet and Co-Flow

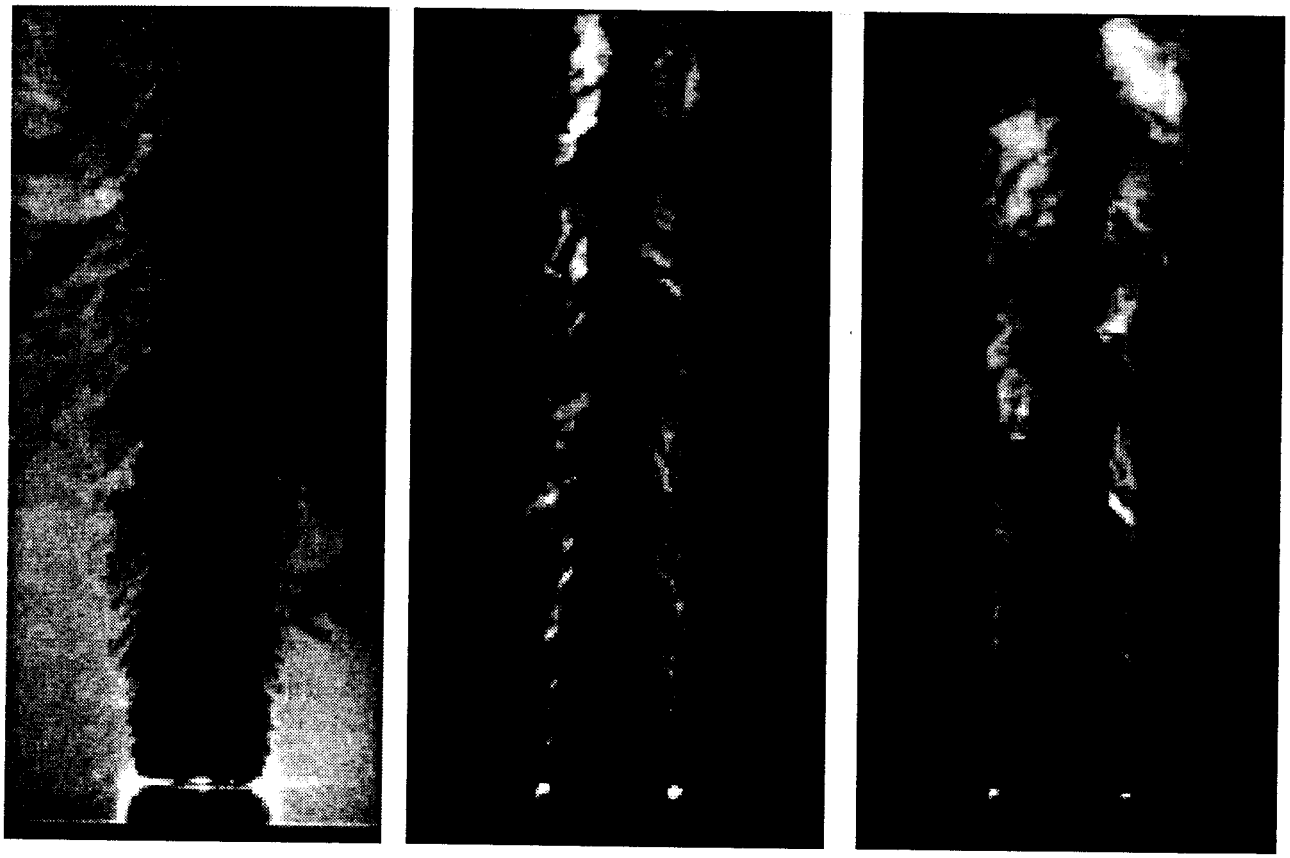

Reference Image
M=0.85 Case

Doppler Image
M=0.85 Case

Doppler Image
NPR for M=1.2 Case

Fig. 7 Mach=0.85 and Mach = 1.2 Compressible Air Jets, SPAHS Seed in Co-Flow Fluid Only

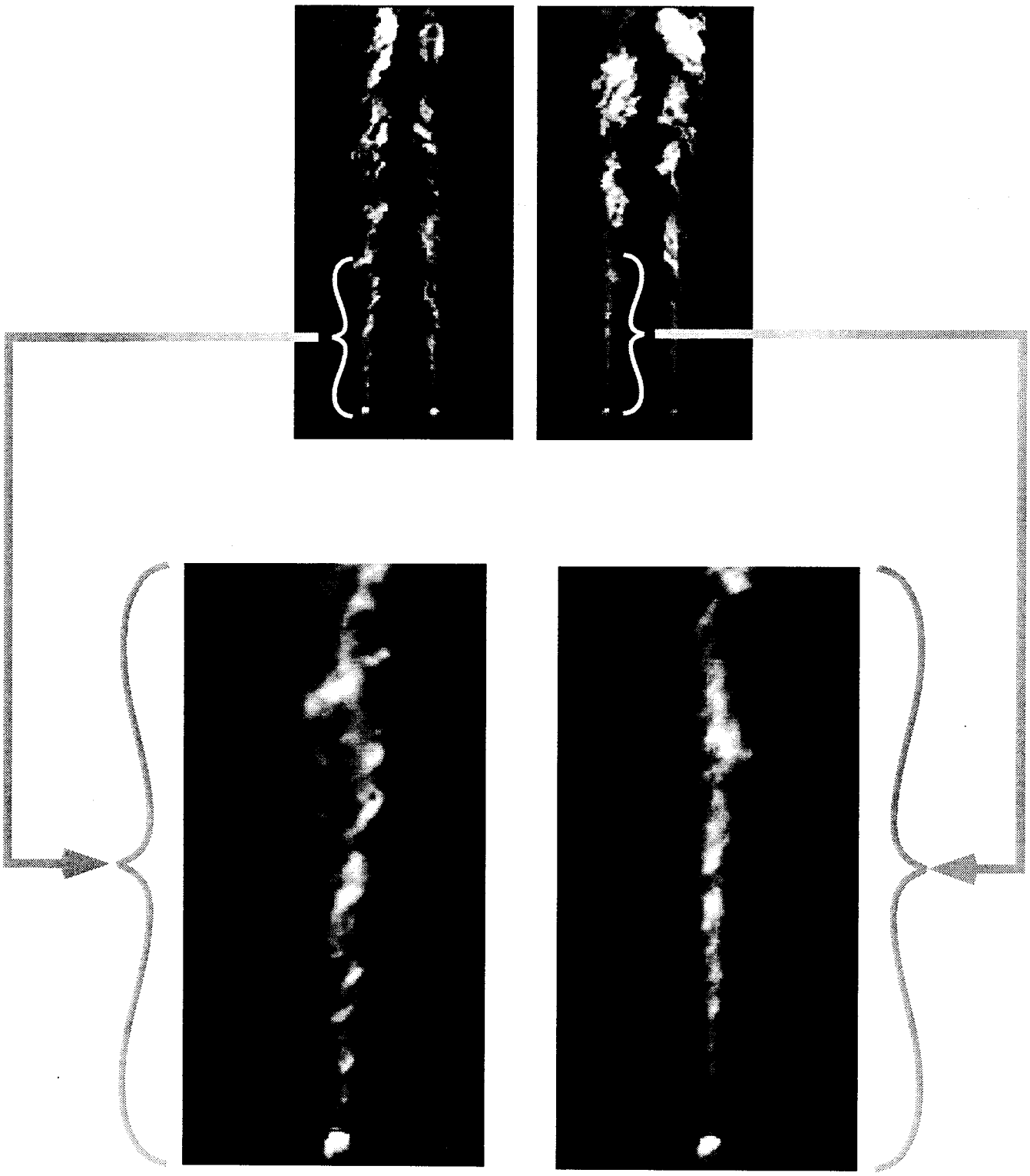


Fig. 8 Initial Shear Layer Structure Comparison: Subsonic/Supersonic

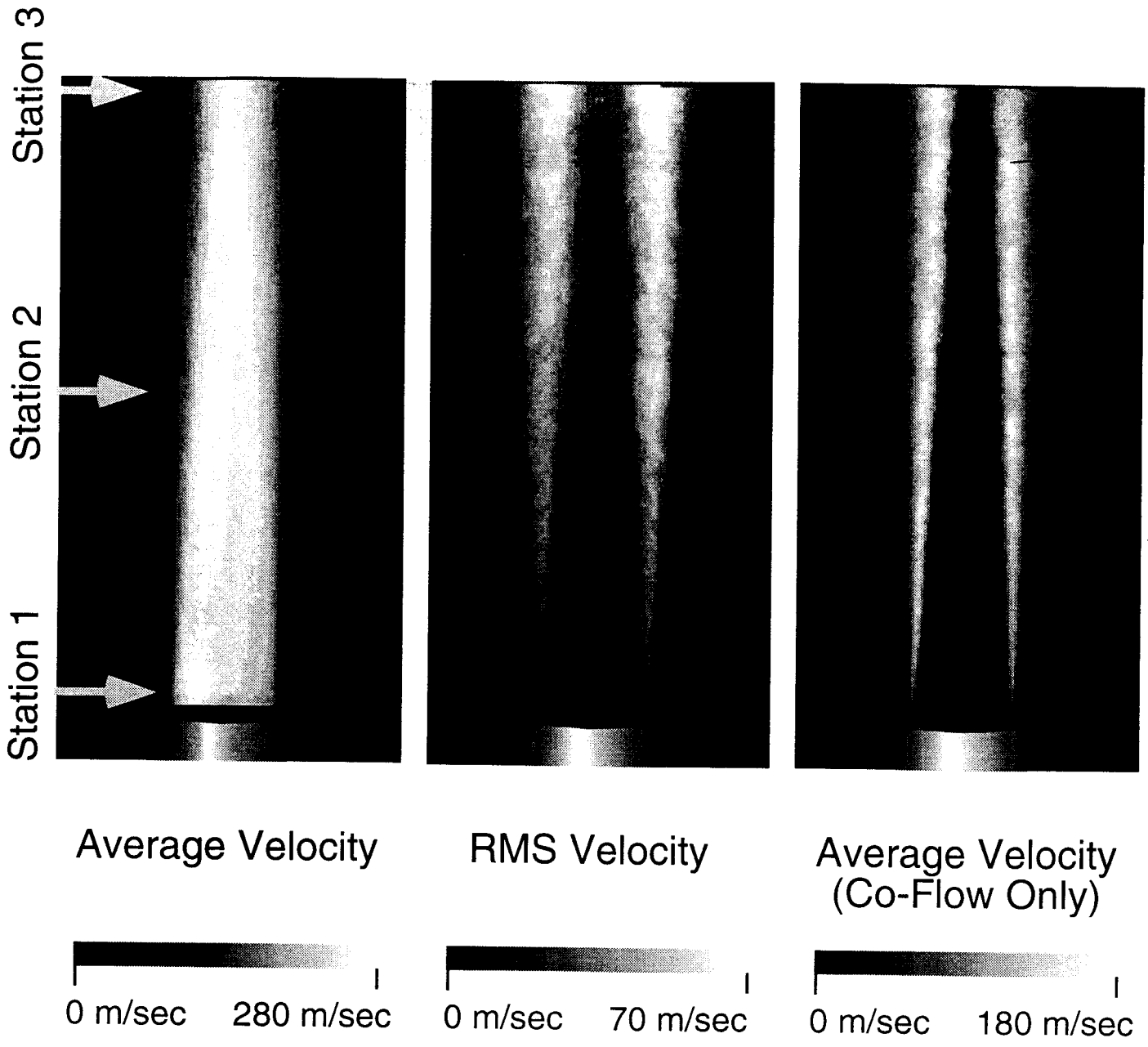


Fig. 9 Mach=0.85 Compressible Air Jet,
240 Frame Statistics

a.) Station 1, 0.52 Radii Downstream

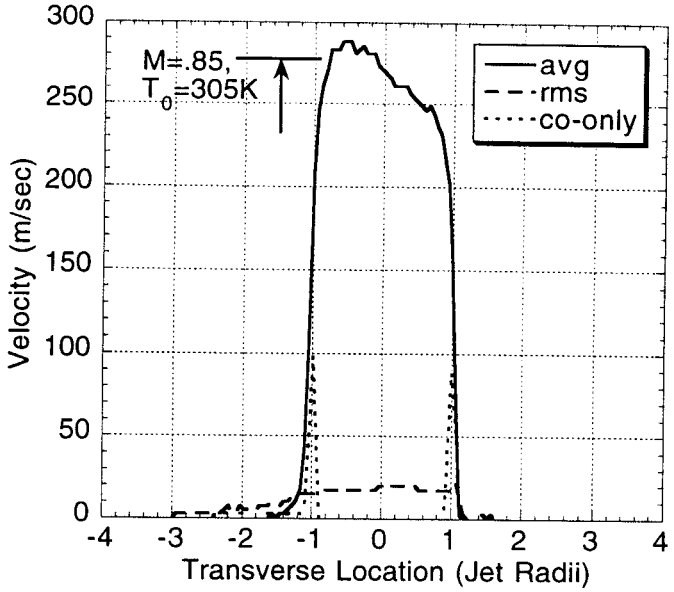


b.) Station 2, 6.6 Radii Downstream

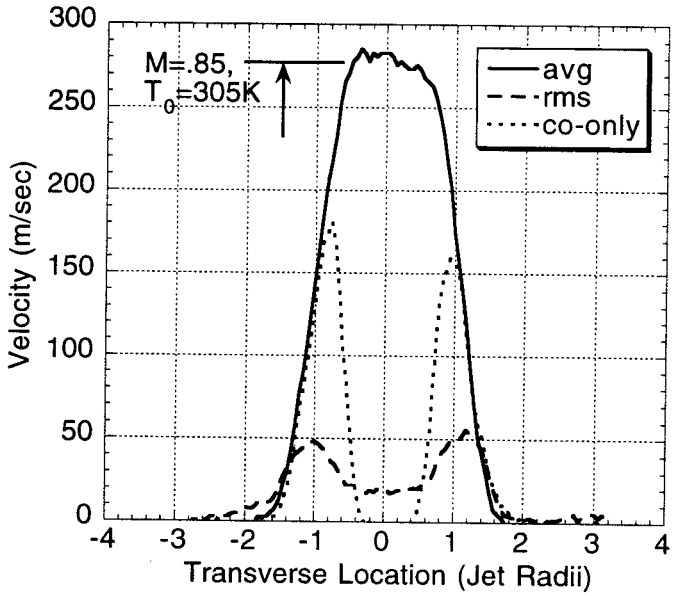


c.) Station 3, 12.7 Radii Downstream

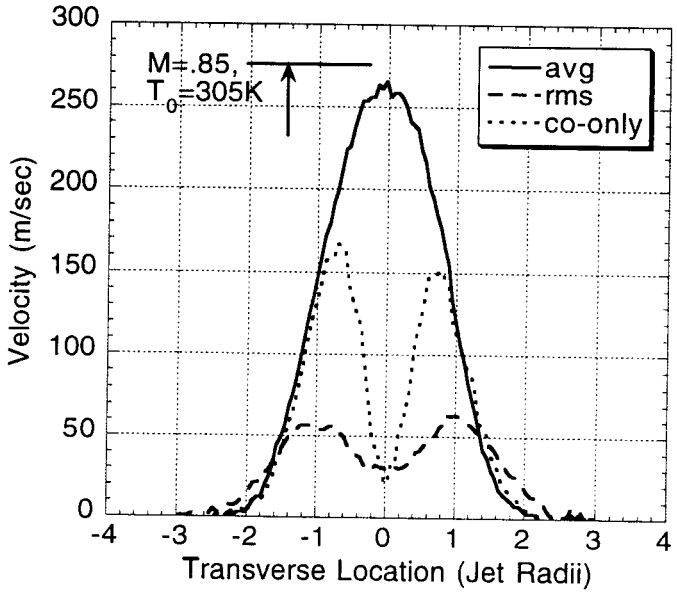


Fig. 10 a-c Selected PDV Velocity Profiles

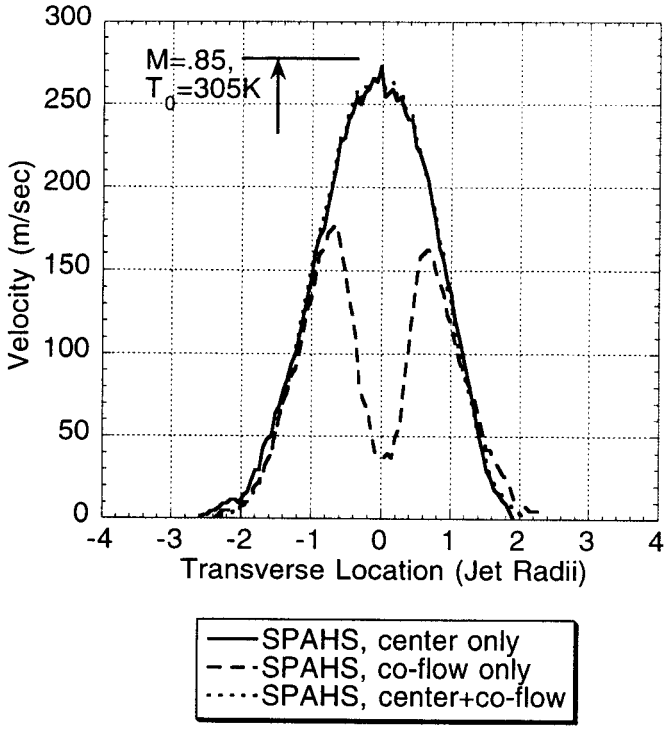


Fig. 11 Comparison Profiles, Seeded Core Flow, Co-Flow, or Both Streams

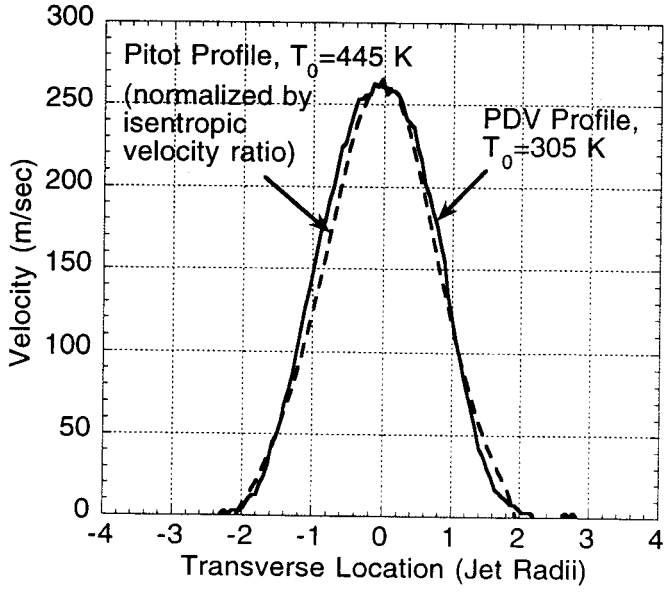


Fig. 12 PDV/Pitot Profiles Comparison